Computational prediction of fracture toughness of polycrystalline metals

Yan Li, David L. McDowell and Min Zhou*

The George W. Woodruff School of Mechanical Engineering,
School of Materials Science and Engineering
Georgia Institute of Technology, Atlanta, GA 30332-0405, U.S.A.

* Corresponding author: min.zhou@me.gatech.edu

Abstract

A three-dimensional multiscale computational framework based on the cohesive finite element method (CFEM) is developed to establish relations between microstructure and the fracture toughness of ductile polycrystalline materials. This framework provides a means for evaluating fracture toughness through explicit simulation of fracture processes involving arbitrary crack paths, including crack-tip microcracking and branching. Fracture toughness is computed for heterogeneous microstructures using the *J*-integral, accounting for the effects of grain size, texture, and competing fracture mechanisms. A rate-dependent, finite strain, crystal plasticity constitutive model is used to represent the behavior of the bulk material. Cohesive elements are embedded both within the grains and along the grain boundaries to resolve material separation processes. Initial anisotropy due to crystallographic texture has a strong influence on inelastic crack tip deformation and fracture toughness. Parametric studies are performed to study the effect of different cohesive model parameters, such as interface strength and cohesive energy, on the competition between transgranular and intergranular fracture. The two primary fracture mechanisms are studied in terms of microstructure characteristics, constituent properties and deformation behaviors. The methodology is useful both for the selection of materials and the design of new materials with tailored properties.

Keywords

cohesive finite element method, crystal plasticity, microstructure-fracture toughness, multiscale framework

1. Introduction

Microstructural design is an important approach for enhancing material properties such as fracture toughness for many industries, including aerospace and automotive engineering. It is of great importance to quantify how an advancing crack interacts with the microstructure at multiple length scales and how microstructure determines a material's fracture toughness through the activation of different fracture mechanisms. A lot of efforts have been made to develop 2D simulation methods to study the crack initiation and propagation in brittle materials (cf. Xu and Needleman [1], Zhai et al. [2] and Li and Zhou [3, 4]) and metallic polycrystalline materials (cf. Guo et al. [5] and Hao et al. [6]). However, fracture is inherently a 3D problem. Most of these 2D models, which assume plane strain conditions, cannot capture the 3D morphologies and orientation of grains, nor do they track crack-material interactions due to non-planar crack extension. This paper aims at expanding the current 2D capabilities to 3D by considering realistic microstructures and incorporating crystalline plasticity in constitutive response modeling. Both intergranular and transgranular fracture modes are

considered in the cohesive finite element method (CFEM) framework developed. This framework also provides a means for evaluating fracture toughness through explicit simulation of 3D fracture processes in microstructures by calculating the *J*-integral.

2. Model structure

Our proposed framework consists of two length scales. At the microscopic scale, 3D cohesive elements with 6-node zero thickness (COH3D6) permeate the whole microstructure as an intrinsic part of material characterization. Constitutive relations for the grains and grain boundaries are specified separately. The cohesive relation allows damage and crack surface separation to be considered. Fracture emerges as a natural outcome of the deformation process without the use of any failure criterion. The macroscopic region is homogenized by using the Mori-Tanaka method. Structural response, such as fracture toughness K_{IC}, is evaluated by calculating the *J*-integral along an arbitrary contour in the homogenized region.

2.1. Generation of 3D polycrystal samples

Voronoi tessellation has been one of the most popular techniques for generating polycrystalline microstructures due to its simplicity, space-filling nature and the availability of theoretical results on the topological properties [7-8]. However, microstructures generated in this way are not always consistent with experimental results [9]. To realistically capture the topological and statistical properties of microstructures, a method for generating a 3D polycrystalline microstructure from a series of 2D images is developed. This capability extends the source of 2D images from computer generated microstructures to realistic section images obtained by Electron Back Scatter Diffraction (EBSD) or Focused Ion Beam (FIB) diffraction. In this paper, the 2D microstructure images are generated by an ellipsoidal packing algorithm [10]. Ellipsoidal grains are randomly placed with the aspect ratios and grain sizes fitted to pre-defined distributions. In order to obtain good delineation of grain boundary and potential crack trajectory, unstructured tetrahedral meshes are generated by iso2mesh [11] as illustrated in Fig. 1.

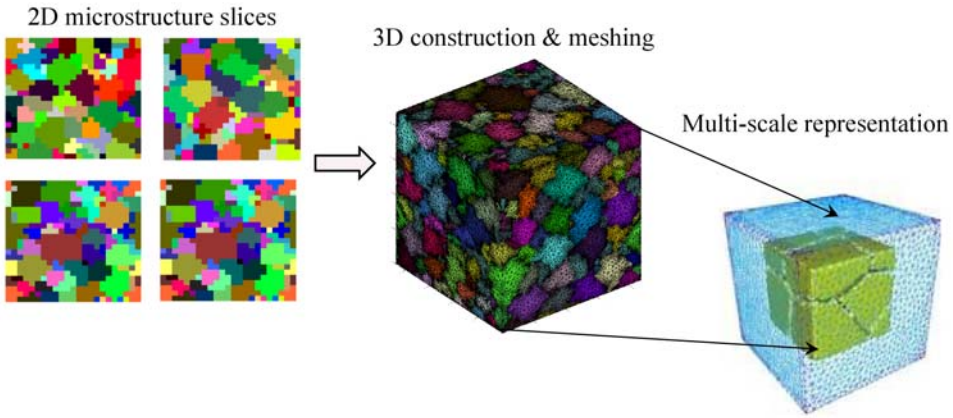

Fig.1 3D microstructure reconstruction and meshing.

2.2. 3D cohesive element insertion

Embedding cohesive surfaces into complicated 3D microstructure meshes is not a trivial task. The biggest challenge lies in how to effectively deal with the changes in the 3D nodal and elemental connectivities due to the introduction of cohesive surfaces. An algorithm has been developed to automatically insert 3D cohesive elements along grain boundaries and within individual grains. The method generally includes the following steps: (1). Find the node set which will be duplicated. The set can be defined as nodes along grain boundaries or within arbitrary grains. (2). Sort out the target elements which include the node set, then duplicate the nodes and redistribute the updated node labels to the corresponding elements. Assign the same coordinates to the duplicated nodes as the virgin nodes. (3). Generate cohesive elements with consistent nodal ordering (clockwise or counter-clockwise) in adjacent element facets. The top and bottom facets are determined by calculating the surface normal. Either top or bottom face can be defined by a positive surface normal value. The key lies in keeping the pattern consistent. (4). Create different cohesive element sets. Sort out cohesive elements that belong to grains or grain boundaries so that different cohesive laws can be correctly assigned.

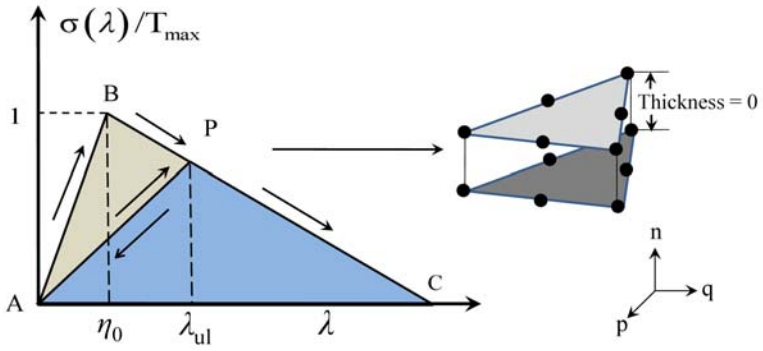

Fig.2 Bilinear traction-separation law.

Both cohesive elements along grain boundaries and within grains follow the bilinear traction-separation law as shown in Fig. 2. This law is derived from a potential Φ which is a function of separation vector Δ through a state variable defined as $\lambda = \sqrt{\left(\Delta_n/\Delta_{nc}\right)^2 + \left(\Delta_t/\Delta_{tc}\right)^2}$. This variable describes the effective instantaneous state of mixed-mode separations. Here, $\Delta_n = \mathbf{n}\cdot\boldsymbol{\Delta}$ and $\Delta_t = \sqrt{\left(\Delta_p\right)^2 + \left(\Delta_q\right)^2} = \sqrt{\left[\left(\boldsymbol{\Delta} - \left(\boldsymbol{\Delta}\cdot\mathbf{n}\right)\mathbf{n}\right)\cdot\mathbf{p}\right]^2 + \left[\left(\boldsymbol{\Delta} - \left(\boldsymbol{\Delta}\cdot\mathbf{n}\right)\mathbf{n}\right)\cdot\mathbf{q}\right]^2}$ = $= \left|\boldsymbol{\Delta} - \left(\boldsymbol{\Delta}\cdot\mathbf{n}\right)\mathbf{n}\right|$ denote, respectively, the normal and tangential components of $\boldsymbol{\Delta}$, with $\mathbf{n}$ being unit normal and $\mathbf{p}$ and $\mathbf{q}$ being two unit tangential vectors. Note that $\mathbf{n}$, $\mathbf{p}$ and $\mathbf{q}$ are mutually perpendicular to each other and form a right-handed triad. Δ_{nc} is the critical normal separation at which the cohesive strength of an interface vanishes under conditions of pure normal

deformation ($\Delta_t = 0$). Similarly, Δ_{tc} is the critical tangential separation at which the cohesive strength of an interface vanishes under conditions of pure shear deformation ($\Delta_n = 0$). $T_{\max}$ represents the maximum traction that the cohesive element can sustain before damage initiates.

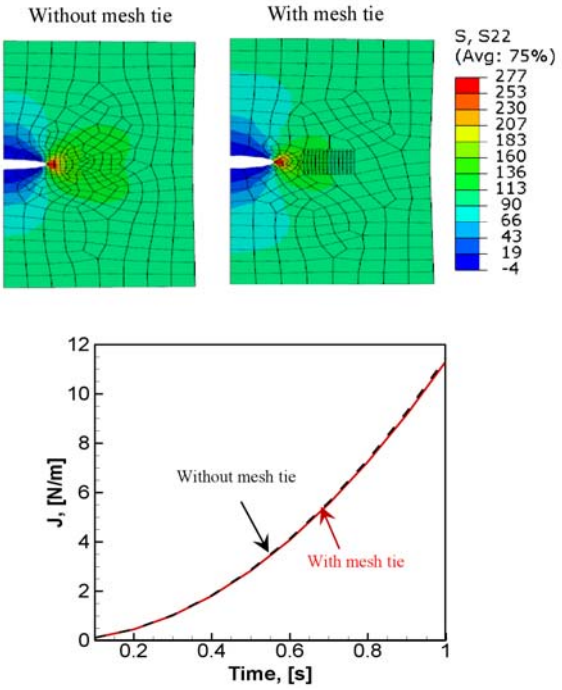

Fig.3 Effect of mesh tie constraint on the calculated J values.

2.3. Generation of mesh tie constraint

Calculation of the *J*-integral in the homogenized region requires a closed contour. It would very difficult to define contours if the homogenized region is meshed with unstructured elements. To solve the problem, two regions of mesh are used. An unstructured tetrahedral mesh is used for the microstructure region and a structured tetrahedral mesh is used for the homogenized region. It would be extremely challenging to create a transitional region that connects the two types of meshes. Instead, the mesh tie constraint in ABAQUS is used. This constraint requires no conformity of node connection between the two regions. It circumvents the problem with acceptable accuracy. As illustrated for a 2D problem in Fig. 3, there is only a very minor difference between the *J* values for cases with and without the mesh tie constraint. It should be noted that iso2mesh cannot generate perfect microstructure meshes with smooth exterior surfaces and sharp vertices as shown in Fig. 4. If the two regions cannot be seamlessly attached, the energy loss caused by the gap will significantly influence the accuracy of calculation. We innovatively develop an algorithm to generate a shell mesh which is around the unsmoothed microstructure block to ensure proper node and element connectivity. The two regions are successfully assembled using the mesh tie constraint as illustrated in Fig. 5.

2.4. Crystal plasticity formulation

Plastic deformation at the macroscopic scale in metals is a manifestation of dislocation motion and interaction at the microscopic scale. The details are intimately related to the basic crystallographic nature of the material as well as the current state of the microstructure. Macroscopic models of plasticity lack the ability to link these fundamental mechanisms to the bulk material response without very substantial experimental characterization. Furthermore, these models give relatively little physical connection between the actual deformation processes and the observed material behavior. Many formulations of constitutive laws for the elastic-plastic deformation of single and polycrystals have long been proposed (cf. Talor [12], Hill and Rice [13], Asaro and Rice [14], Peire et al. [15] and McGinty and McDowell [16]). The basic premise of these theories is that macroscopic plastic deformation is related to the cumulative process of slip (or twin) system shearing relative to the lattice. This methodology provides a physical link between the processes at radically different length scales. The two basic components of crystal plasticity model are the kinematic and kinetic relations. The kinematic relations provide the mathematical framework for describing the physical process of dislocation motion based on continuum deformation fields, whereas the kinetic relations incorporate the material and/or mechanism dependence of non-equilibrium dislocation motion and interaction.

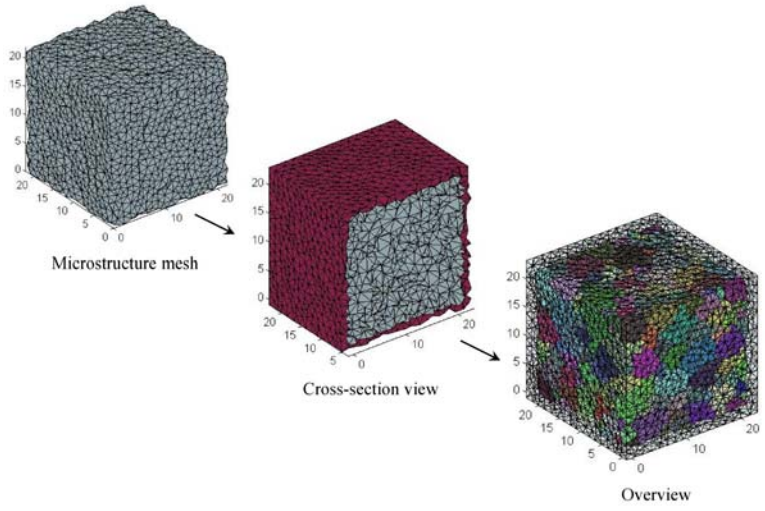

Fig. 4 Shell mesh region around the unsmoothed microstructure mesh.

The multiplicative decomposition of the total deformation gradient is given by

$$\mathbf{F} = \mathbf{F}^e \cdot \mathbf{F}^p, \tag{1}$$

where $\mathbf{F}^e$ is the elastic deformation gradient representing the elastic stretch and rotation of lattice, and $\mathbf{F}^p$ is the plastic deformation gradient describing the collective effects of dislocation motion along the active slip planes relative to a fixed lattice in the reference configuration. Unit vectors $\boldsymbol{s}_0^\alpha$

and $\boldsymbol{n}_0^\alpha$ denote the slip direction and the slip plane normal direction, respectively for the α^{th} slip system in the undeformed configuration. The resolved shear stress on each slip system is related to the Cauchy stress tensor $\boldsymbol{\sigma}$ according to

$$\tau^\alpha = \boldsymbol{\sigma}:\left(\boldsymbol{s}^\alpha \otimes \boldsymbol{n}^\alpha\right), \tag{2}$$

where the slip vectors have been rotated into the current configuration. Under the application of the resolved shear stress, the shearing rates $\dot{\gamma}^\alpha$ on the slip systems are related to the plastic velocity gradient in the intermediate configuration according to

$$\mathbf{L}^p = \sum_\alpha \dot{\gamma}^\alpha \, \mathbf{s}_0^\alpha \otimes \mathbf{n}_0^\alpha, \tag{3}$$

with $\dot{\gamma}^\alpha$ ascribed to follow the rate-dependent flow rule as

$$\dot{\gamma}^\alpha = \dot{\gamma}_0 \left\langle \frac{\tau^\alpha - \chi^\alpha}{g^\alpha} \right\rangle^m \operatorname{sgn}\left(\tau^\alpha - \chi^\alpha\right), \tag{4}$$

where m is the reverse strain rate sensitivity exponent and g^α and χ^α are drag stress and back stress, respectively on the α^{th} slip system. These quantities evolve according to

$$\begin{cases} \dot{g}^\alpha = H \sum_{\beta=1} q^{\alpha\beta} \left|\dot{\gamma}^\beta\right|, \text{ and} \\ \dot{\chi}^\alpha = A_{kin}\dot{\gamma}^\alpha - A_{dyn}\chi^\alpha \left|\dot{\chi}^\alpha\right|. \end{cases} \tag{5}$$

Here $q^{\alpha\beta}$ is the latent hardening coefficient, H, A_{kin} and A_{dyn} are the isotropic hardening, kinematic hardening and dynamic recovery coefficients, respectively. These non-linear coupled differential equations are solved via the fourth order Runge-Kutta integration scheme using VUMAT.

3. Conclusion

A cohesive finite element based multi-scale framework is developed to simulate crack initiation and propagation in 3D polycrystalline microstructures. Crystal plasticity is incorporated into the constitutive relations so as to capture how anisotropic deformation and texture evolution affect

crack propagation and the activation of different fracture mechanisms. The methodology is useful both for the selection of materials and the design of new materials with tailored properties.

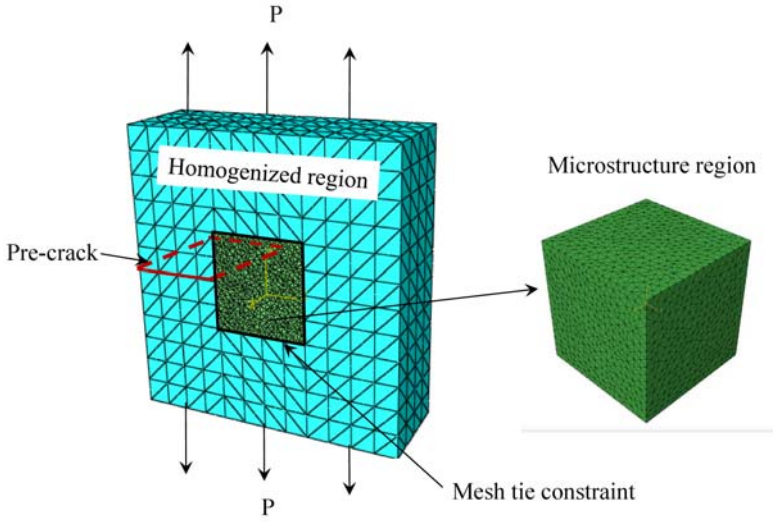

Fig. 5 Model assembly between microstructure and homogenized region by mesh tie.

Acknowledgements

This research is primarily supported by the NSF Center for Computational Materials Design (CCMD) at Georgia Institute of Technology and Pennsylvania State University. MZ also acknowledges support from the National Research Foundation of Korea through WCU Grant No. R31-2009-000-10083-0.

References

[1] X. P. Xu and A. Needleman, "Numerical Simulations of Fast Crack-Growth in Brittle Solids," *J. Mech. Phys. Solids*, vol. 42, p. 1397, Sep 1994.

[2] J. Zhai, V. Tomar, and M. Zhou, "Micromechanical simulation of dynamic fracture using the cohesive finite element method," *Journal of Engineering Materials and Technology*, vol. 126, pp. 179-191, Apr 2004.

[3] Y. Li and M. Zhou, "Prediction of fracture toughness of ceramic composites as function of microstructure: I. Numerical simulations," *Journal of the Mechanics and Physics of Solids*, vol. 61, pp. 472-488, 2013.

[4] Y. Li and M. Zhou, "Prediction of fracturess toughness of ceramic composites as function of microstructure: II. analytical model," *Journal of the Mechanics and Physics of Solids*, vol. 61, pp. 489-503, 2013.

[5] X. Guo, K. Chang, L. Q. Chen, and M. Zhou, "Determination of fracture toughness of AZ31 Mg alloy using the cohesive finite element method," *Engineering Fracture Mechanics*, vol. 96, pp. 401-415, 2012.

[6] S. Hao, H. Lin, R. R. Binomiemi, D. M. G. Combs, and G. Fett, "A multi-scale model of

intergranular fracture and computer simulation of fracture toughness of a carburized steel," *Computational Materials Science,* vol. 48, pp. 241-249, 2010.

[7] A. Leonardi, P. Scardi, and M. Leoni, "Realistic nano-polycrystalline microstructures: beyond the classical Voronoi tessellation," *Philosophical Magazine,* vol. 92, pp. 986-1005, 2012/03/11 2012.

[8] T. Luther and C. Könke, "Polycrystal models for the analysis of intergranular crack growth in metallic materials," *Engineering Fracture Mechanics,* vol. 76, pp. 2332-2343, 2009.

[9] T. Xu and M. Li, "Topological and statistical properties of a constrained Voronoi tessellation," *Philosophical Magazine,* vol. 89, pp. 349-374, 2009/02/01 2009.

[10] C. P. Przybyla and D. L. McDowell, "Simulation-based extreme value marked correlations in fatigue of advanced engineering alloys," *Procedia Engineering,* vol. 2, pp. 1045-1056, 2010.

[11] F. Qianqian and D. A. Boas, "Tetrahedral mesh generation from volumetric binary and grayscale images," in *Biomedical Imaging: From Nano to Macro, 2009. ISBI '09. IEEE International Symposium on*, 2009, pp. 1142-1145.

[12] G. I. Taylor, "Plastic strain in metals.," *Journal of the Institute of Metals,* vol. 62, pp. 307-324, 1938.

[13] R. Hill and J. R. Rice, "Constitutive analysis of elastic-plastic crystals at arbitrary strain," *Journal of the Mechanics and Physics of Solids,* vol. 20, pp. 401-413, 1972.

[14] R. J. Asaro and J. R. Rice, "Strain Localization in Ductile Single-Crystals," *Journal of the Mechanics and Physics of Solids,* vol. 25, pp. 309-338, 1977.

[15] D. Peirce, R. J. Asaro, and A. Needleman, "An Analysis of Nonuniform and Localized Deformation in Ductile Single-Crystals," *Acta Metallurgica,* vol. 30, pp. 1087-1119, 1982.

[16] R. D. McGinty and D. L. McDowell, "Application of multiscale crystal plasticity models to forming limit diagrams," *Journal of Engineering Materials and Technology-Transactions of the Asme,* vol. 126, pp. 285-291, Jul 2004.